JOURNAL OF AIRCRAFT
Vol. 36, No. 2, March–April 1999

Experimental and Theoretical Correlation of Helicopter Rotor Blade–Droop Stop Impacts

Jonathan A. Keller* and Edward C. Smith†
Pennsylvania State University, University Park, Pennsylvania 16802-1401

The transient response of a nonrotating articulated rotor blade undergoing a droop stop impact is examined. The rotor blade is modeled using the finite element method, and the droop stop is simulated using a conditional rotational spring. No aerodynamic effects are modeled. Three methods of time integrating the equations of motion were studied: 1) a direct integration of the full finite element space equations of motion; 2) a modal space integration using only hinged modes; and 3) a modal space integration using either hinged or cantilevered modes, depending on blade/droop stop contact. Given a range of initial flap hinge angles, drop tests of a one-eighth Froude-scaled articulated model rotor blade were conducted at zero rotational speed. The transient tip deflection, flap hinge angle, and strain were measured, and they displayed good correlation with all three analytic methods. Modal parameter identification tests were performed on the model blade to determine its natural frequencies and damping ratios for both hinged and cantilevered conditions. The measured structural damping was shown to significantly improve correlation between the experimental and analytic results. Computational efficiency for the problem under consideration was not of serious concern. However, in a comprehensive aeroelastic analysis, it was found that a modal space integration using either hinged or cantilevered modes, depending on blade/droop stop contact, reduced computational time by two orders of magnitude.

Nomenclature

A = blade cross-sectional area
C = global damping matrix
E = modulus of elasticity
e = flap hinge offset
$\boldsymbol{F}$ = global load vector
$\boldsymbol{H}$ = vector of Hermitian shape functions
h = blade thickness
I = area moment of inertia
$\tilde{I}$ = identity matrix
K = global stiffness matrix
K_β = droop stop spring stiffness
L = blade length
M = global mass matrix
q = modal amplitudes
s = blade-deformed length coordinate
T = kinetic energy
t = time
U = strain energy
W = external work
$w, \tilde{w}$ = flapping deflections
α = proportional damping constant
β_{hinge} = flap hinge angle
ζ = modal damping ratio
η = proportional damping constant
ρ_s = blade mass density
Φ = mode shape
ω = blade natural frequency
$\cdot$ = $\partial(\,)/\partial t$
$-$ = modal space quantity

Subscripts
B = contribution from blade
c = cantilevered condition
DS = contribution from droop stop
h = hinged condition
NL = contribution from nonlinear effects
SD = static deflection

Received May 17, 1998; revision received Sept. 15, 1998; accepted for publication Sept. 16, 1998.

*Rotorcraft Fellow, Department of Aerospace Engineering, 233 Hammond Building. Student Member AIAA.

†Associate Professor, Department of Aerospace Engineering, 233 Hammond Building. Member AIAA.

Introduction

UNIQUE problems can often be encountered when rotorcraft are operated from ship-based platforms. One such problem can occur during the engagement or disengagement of the rotor system while the rotor is spinning at very low speeds. High aerodynamic forces caused by high winds combined with low centrifugal stiffening at low rotor speeds can result in excessive aeroelastic flapping of the rotor. If the flapping becomes large enough, the blade tips can contact the fuselage of the helicopter. This contact is called a tunnel strike for tandem rotor configurations, and a tailboom strike for single rotor configurations. Tailboom and tunnel strikes have been the subject of both analytical and experimental investigation in Refs. 1–9.

The H-46 Sea Knight, a tandem rotor helicopter with articulated rotor blades, is particularly susceptible to tunnel strikes.[10–12] Over 100 H-46 tunnel-strike incidents, most often occurring at less than 20% of full rotor speed, were reported from 1964 to 1989.[13] The majority of tunnel strikes caused minor damage to the helicopter; however, several caused major damage to the airframe, resulting in the complete loss of the helicopter. Large blade and hub loads are also a source of concern when excessive flapping of the rotor occurs. In adverse weather, the conditions in which the rotor can be safely engaged or disengaged must be restricted, which severely limits the operational capability of the helicopter and its usefulness to the fleet. For example, a helicopter can only operate from a frigate in the North Sea an average of 10% of the time in winter.[14]

One important feature of articulated, i.e., hinged, rotor blades is the droop stop mechanism. The droop stop, typically located near the flap hinge of the blade, supports the blade weight by preventing the downward rotation of the flap hinge while the rotor system is at rest and at low speeds. During the engagement and disengagement of the rotor system, excessive

flapping can cause the rotor blade to repeatedly impact the droop stop. The boundary conditions of the blade change dramatically during such an event. When the blade is not in contact with the droop stop, the flap hinge is free to rotate, and the blade acts as a hinged beam. When the blade is in contact with the droop stop, the flap hinge is restrained from further downward rotation, and the blade acts as a cantilevered beam. A high-rate spring is typically used to analytically model the droop stop, effectively freezing the hinge angle during an impact.[3-9]

Leone[15] derived the bending moment distribution along an articulated rotor blade during an impact using only the fundamental cantilevered mode of the blade. Using a full-scale aircraft operating at full rotor speed, an excessive cyclic pitch input to the rotor system was used to cause an impact between the rotor blade and droop stop. Measurements of the root bending moment for varying blade flap impact velocities were recorded with an oscilloscope, and agreed well with the predicted values.

A significant amount of research exists that focuses on the impact of elastic bodies with rigid constraints. The response of such structures is normally calculated using the mode shapes of the structure. If this procedure is followed, the constraint can be treated in one of two approaches.

In the first approach to treating impacts, the motion can be described in terms of the modes of the unconstrained structure and the constraint treated as an applied force. This is the method used in the transient aeroelastic analyses in Refs. 3–9, and has also been applied to similar problems. Fathi and Popplewell[16] and Lo[17] studied a cantilever beam contacting a rigid stop. Using only the unconstrained modes, Lo compared the analytical predictions of the beam motion with the photographically measured beam motion using a multiflash strobe light and an oscilloscope, and found good agreement. Molnar et al.[18] and Shah et al.[19] considered the problem of the response of gap-restrained piping systems using only the unconstrained modes of the system. Significant time savings were realized using the modal superposition method to integrate the equations of motion. Davies and Rogers[20] compared the frequency responses of the free end of a cantilevered beam contacting a rigid linear stop using either only the unconstrained or only the constrained mode shapes. The constrained mode shapes were obtained in terms of the unconstrained modes and were shown to be orthogonal. In addition, the unconstrained modes were proven to form a complete set of modes for the constrained structure.

In the second approach to treating impacts, the unconstrained modes can be used to describe the motion when not in contact with the restraint, and the constrained modes can be used to describe the motion when in contact with the restraint. Chen et al.[21] used this method to describe the vibration of a simply supported beam constrained between two rigid stops, and to calculate the steady-state deflection and dynamic stresses in the beam. Rogers and Pick[22,23] presented finite element approaches to the problem of a heat-exchanger tube vibrating inside an annulus, and compared the simulated and experimentally measured vibration response of the beam. Shaw[24] examined a cantilevered beam contacting a rigid stop, and compared the measured and predicted subharmonic resonances, period doublings, and chaotic behavior.

The objective of the current research is to analytically predict and experimentally measure the transient response of a Froude-scaled model articulated rotor blade undergoing a series of droop stop impact events. Specifically, the finite element method is used to model the blade, and three time integration schemes are employed to calculate the transient response of the beam.

Derivation of the Blade Equations of Motion

A schematic diagram of the elastic blade and coordinate system is shown in Fig. 1. The equations governing the transverse

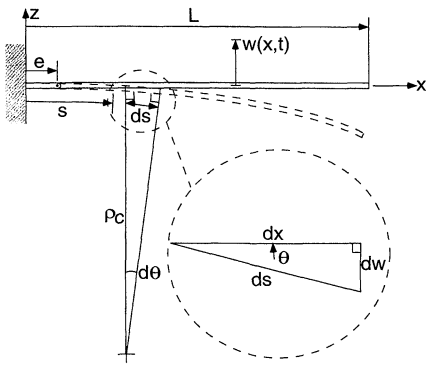

Fig. 1 Beam coordinate system.

motion of the elastic blade are derived using the generalized Hamilton's principle:

$$\delta\Pi = \int_{t_1}^{t_2} (\delta T - \delta U + \delta W)\, dt = 0 \tag{1}$$

The variation of the kinetic energy of the blade is

$$\delta T = \int_0^L \int \int_A \rho_s \dot{w} \delta \dot{w}\, dA\, ds \tag{2}$$

The variation of the strain energy can be expressed as a summation of the contributions from the elastic bending of the rotor blade and the deformation of the droop stop spring:

$$\delta U = \delta U_B + \delta U_{DS} \tag{3}$$

Because the largest tip deflections to be explored in this study were to be 18% of the length of the beam, a nonlinear beam bending theory was utilized in the formulation of the blade strain energy caused by elastic bending. From Ref. 25, the strain energy is

$$U_B = \frac{1}{2}\int_0^L EI \left(\frac{\partial^2 w}{\partial s^2}\right)^2 \left[1 + \left(\frac{\partial w}{\partial s}\right)^2 + \left(\frac{\partial w}{\partial s}\right)^4 + \left(\frac{\partial w}{\partial s}\right)^6 + \cdots\right] ds \tag{4}$$

Taking the variation of Eq. (4) yields

$$\delta U_B = \int_0^L EI \left(\frac{\partial^2 w}{\partial s^2}\right) \delta \left(\frac{\partial^2 w}{\partial s^2}\right) ds + \delta U_{B_{NL}} \tag{5}$$

The complete derivation of the nonlinear terms is presented in Ref. 26. The analysis uses a conditionally applied rotational spring, based on the instantaneous value of the hinge angle to model the droop stop. The variation of the droop stop strain energy is

$$\delta U_{DS} = K_\beta(t)(\beta_{hinge} - \beta_{DS})\delta\beta_{hinge} \tag{6}$$

The hinge angle is calculated directly from the difference in the slope of the blade on either side of the flap hinge. For hinge angles above the specified impact angle, the spring stiffness is zero. For hinge angles equal to or below the specified impact angle, the spring stiffness is set large enough to restrain the hinge angle to less than 0.001 deg of rotation. To meet this requirement, it was necessary to set the spring stiffness to one million times the static weight moment of the blade about the flap hinge:

$$\begin{aligned} K_\beta(t) &= 0 \quad \text{if} \quad \beta_{hinge} > \beta_{DS} \quad \text{(hinged)} \\ K_\beta(t) &= 1 \times 10^6 \int_e^L mgs\, ds \quad \text{if} \quad \beta_{hinge} \le \beta_{DS} \quad \text{(cantilevered)} \end{aligned} \tag{7}$$

Aerodynamic forces have been neglected in this study because the rotational speed is zero. The variation of the external work is then simply from gravitational forces:

$$\delta W = -g \int_0^L \int \int_A \rho_s \, dA \delta w \, ds \tag{8}$$

The energy expressions are spatially discretized using the finite element method. Cubic Hermitian shape functions are used to expand the flapping degrees of freedom:

$$w(s, t) = \boldsymbol{H}(s)\tilde{w}(t) \tag{9}$$

Summation of the elemental matrices and vectors yields the global form of the virtual energy expression:

$$\delta\Pi = \int_{t_1}^{t_2} \delta\tilde{w}[M\ddot{\tilde{w}} + K\tilde{w} + \boldsymbol{F}_{\mathrm{NL}}(\tilde{w}) - \boldsymbol{F}] \, dt = 0 \tag{10}$$

Note the nonlinear terms from the blade strain energy equation have been expressed in terms of a nonlinear forcing vector. Special attention must be taken at the flap hinge location because two distinct rotational degrees of freedom exist. Motion dependent and independent terms from Eq. (6) must be included in K and $\boldsymbol{F}$, respectively. Because the droop stop stiffness can change, depending on the flap hinge angle, two different K and $\boldsymbol{F}$ are used:

$$\begin{aligned} K &= K_h \quad \text{and} \quad \boldsymbol{F} = \boldsymbol{F}_h \quad \text{if} \quad \beta_{\text{hinge}} > \beta_{\text{DS}} \\ K &= K_c \quad \text{and} \quad \boldsymbol{F} = \boldsymbol{F}_c \quad \text{if} \quad \beta_{\text{hinge}} \leq \beta_{\text{DS}} \end{aligned} \tag{11}$$

If a proportional damping model is chosen, the global damping matrix is

$$C = \alpha M + \eta K \tag{12}$$

The global equations of motion are then

$$M\ddot{\tilde{w}} + C\dot{\tilde{w}} + K\tilde{w} = \boldsymbol{F} - \boldsymbol{F}_{\mathrm{NL}}(\tilde{w}) \tag{13}$$

The blade tip deflection and the flap hinge angle are simply calculated from the appropriate degrees of freedom. The strain is calculated from

$$\varepsilon_{ss}(s, t) = [(-h)/2]\boldsymbol{H}''(s)\tilde{w}(t) \tag{14}$$

Analysis

For computational efficiency, it is common to transform the global equations of motion into a modal coordinate system:

$$\tilde{w} \cong \Phi(s)q(t) \tag{15}$$

Substitution of Eq. (15) into Eq. (13), and multiplication by Φ^T, yields an uncoupled set of equations because aerodynamic effects have been neglected and the modes are orthogonal:

$$\bar{M}\ddot{q} + \bar{C}\dot{q} + \bar{K}q = \bar{\boldsymbol{F}} - \bar{\boldsymbol{F}}_{\mathrm{NL}}(\tilde{w}) \tag{16}$$

If the mode shapes are also mass normalized,

$$\begin{aligned} &\bar{M} = \tilde{I}, \quad \bar{C} = (2\zeta\omega), \quad \bar{K} = (\omega^2) \\ &\bar{\boldsymbol{F}} = \Phi^T\boldsymbol{F}, \quad \bar{\boldsymbol{F}}_{\mathrm{NL}}(\tilde{w}) = \Phi^T\boldsymbol{F}_{\mathrm{NL}}(\tilde{w}) \end{aligned} \tag{17}$$

Recall that two different stiffness matrices are used in this transient analysis: one corresponding to the cantilevered condition of the beam, and one corresponding to the hinged condition of the beam. Therefore, two independent sets of natural frequencies and mode shapes are generated:

$$\begin{aligned} \omega &= \omega_h \quad \text{and} \quad \Phi = \Phi_h \quad \text{if} \quad \beta > \beta_{\text{hinge}} \\ \omega &= \omega_c \quad \text{and} \quad \Phi = \Phi_c \quad \text{if} \quad \beta \leq \beta_{\text{hinge}} \end{aligned} \tag{18}$$

In this particular study, the equations of motion can be solved using three different techniques. In each method, the high-rate rotational spring, $K_\beta(t)$, must be added to or removed from the equations of motion, depending on blade-droop stop contact. In all three techniques, the Newmark time-integration method[27] was used to time integrate the resulting equations of motion. The first and simplest technique is a direct solution of Eq. (13), called a full finite element space integration. The second technique is a solution of Eq. (16), using only the hinged modes of the beam, regardless of blade-droop stop contact, called a modal swapping off integration. The third and most complicated technique is a solution of Eq. (16), using either the hinged or cantilevered modes, depending on droop stop contact, called a modal swapping on integration. In this method, the modal amplitudes must be adjusted to maintain the physical shape of the beam when the mode shapes are changed, or discontinuities can arise in the solution.[26,28] To accomplish this, the following procedure is followed.[28] The deflection of the beam can be approximated by either set of modal matrices and modal amplitudes:

$$\tilde{w} \cong \Phi_h q_h \cong \Phi_c q_c \tag{19}$$

During a transient analysis, when the calculated hinge angle becomes equal to or goes below the droop stop angle, a switch from hinged mode shapes to cantilevered mode shapes is performed. In addition, the modal amplitudes must be adjusted. Premultiplying Eq. (19) by $\Phi_c^T M$ yields

$$\Phi_c^T M \Phi_c q_c = \Phi_c^T M \Phi_h q_h \tag{20}$$

Because the mode shapes have previously been mass normalized, $\Phi_c^T M \Phi_c = \tilde{I}$, and

$$q_c = \Phi_c^T M \Phi_h q_h \tag{21}$$

Similarly, when the calculated hinge angle rises above the droop stop angle, a switch from the cantilevered mode shapes to the hinged mode shapes is performed, and the modal amplitudes must be readjusted:

$$q_h = \Phi_h^T M \Phi_c q_c \tag{22}$$

Experiment

A Froude-scaled structural model of an H-46 rotor blade was constructed from 6061-T6 aluminum. The mass and flapwise stiffness distributions of both the model and the H-46 blades can be found in Refs. 26 and 28. The mass and stiffness distributions of the model blade were matched as closely as possible to the H-46 blade, to ensure that the vibration behavior of the two blades is similar. The length of the H-46 blade is 25.5 ft, and the length of the model blade is 3.3 ft.

Modal Analysis Tests

Experimental modal analysis tests were performed on the model blade to determine its natural frequencies and modal damping ratios for the first six modes in both hinged and cantilevered states. Frequency response functions were collected using WAVEPAK® data acquisition software, and were analyzed using STARModal® software. Complete details and results from the modal analysis tests are included in Ref. 26.

The natural frequencies calculated in the finite element analysis of the beam and measured in the modal analysis tests are presented along with the measured modal damping ratios in

Table 1 Experimental modal analysis results

	Hinged				Cantilevered			
Mode	Predicted ω_n, Hz	Measured ω_n, Hz	Error, %	Measured ζ, % ζ_{crit}	Predicted ω_n, Hz	Measured ω_n, Hz	Error, %	Measured ζ, % ζ_{crit}
1	0.0	——[a]	——[a]	——[a]	3.0	3.1	3.2	0.0
2	9.3	9.3	0.0	4.5	19.9	19.2	3.6	0.4
3	28.4	27.3	4.0	0.9	57.3	55.1	4.0	0.9
4	64.7	61.3	5.5	0.2	111.9	107.9	3.7	3.9
5	121.8	116.6	4.5	0.3	165.3	198.6	16.8	0.7
6	199.5	189.8	5.1	0.6	211.5	246.8	14.3	0.0

[a]Not measurable in WAVEPAK®.

Table 1. In general, there is good agreement between the finite element results and the modal analysis tests. All of the measured natural frequencies, except for the fifth and sixth cantilevered modes, were within 5% of the predicted natural frequencies. The measured modal damping ratios in Table 1 are used in both the modal swapping off and modal swapping on time integrations.

Drop Test Procedure

To focus on the impact between the rotor blade and the droop stop, a series of nonrotating drop tests were conducted. The procedure for each drop test is described as follows. The root end of the blade was clamped between vice grips. Then the section of the blade outboard of the flap hinge was rotated upward and given an initial flap hinge angle, ranging from 2 to 10 deg. Once the desired flap hinge angle was reached, the blade was held in place by an electromagnet located just beyond the flap hinge.

Each drop test commenced when the electromagnet was shut off. Without anything to support it, the blade section outboard of the flap hinge rotated downward about the flap hinge until it contacted the droop stop, set at an angle of 0 deg. At this point, the blade's inertia caused it to elastically bend. Once the blade reached its point of maximum downward deflection, its excess strain energy is reconverted into kinetic energy and the blade rebounds upward. The motion of the blade was measured for one full cycle of downward bending and upward rebounding. This process was repeated four times for each initial flap hinge angle to determine the repeatability of the data.

Instrumentation

A schematic of the model blade and the measurement devices is shown in Fig. 2. An accelerometer, rated at $\pm 50g$, was attached to the blade tip. Three strain gauges were attached to the upper surface of the model blade at locations 20, 30, and 40% of the total blade length. A linear motion potentiometer was located just outboard of the flap hinge. The accelerometer had a calibration constant of 109 mV/g and the strain gauges were calibrated through an electric shunt. The linear motion potentiometer was calibrated by manually lifting the blade to a known flap hinge angle, which was measured with a protractor, and recording the resulting voltages from the MEPTS-9000 system. It is estimated that this process was accurate to within ± 1 deg.

At the beginning of each drop test, the initial shape of the beam is a combination of the static droop under its own weight and a known rotation of the flap hinge, shown in Fig. 2. The initial condition for the tip deflection is given by

$$w_{tip}(t = 0) = (L - e)\sin[\beta_{hinge}(t = 0)] + w_{sd} \tag{23}$$

Because no direct measurement of the static tip deflection was readily available, it was assumed to be exactly the same as predicted by the finite element model. The initial velocity was set equal to zero because the blade was released from rest. Once the initial position and velocity of the blade tip were

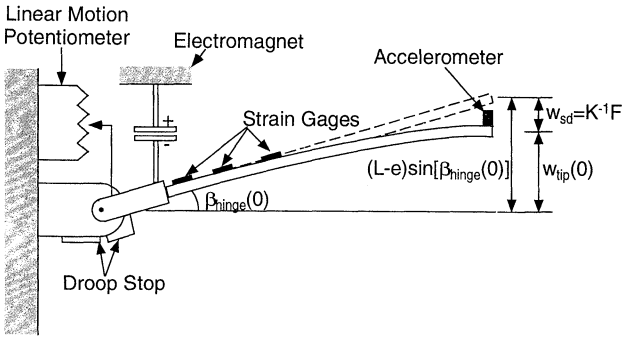

Fig. 2 Model blade schematic.

specified, the measured tip accelerations can be used to calculate the measured tip displacement and tip velocity:

$$\begin{aligned} \dot{w}(t) &= (\Delta t/2)[\dot{w}_{tip}(t) + \dot{w}_{tip}(t - \Delta t)] \\ w(t) &= (\Delta t/2)[\dot{w}_{tip}(t) + \dot{w}_{tip}(t - \Delta t)] \end{aligned} \tag{24}$$

Some error in each tip acceleration measurement exists. When integrated twice in time, this error can have a measurable impact on the tip deflections. Upon further investigation, a ± 5 mV oscillation in the accelerometer signal was identified, even when placed upon a motionless table. As stated earlier, the calibration constant for the accelerometer was 109 mV/g; therefore, the ± 5 mV drift translates into an uncertainty of $\pm 0.046g$ in the acceleration measurement. To estimate the impact of this uncertainty in the acceleration measurement, the equation for the additional displacement, owing only to this drift, is given by

$$\Delta w(t) = \tfrac{1}{2}\Delta a t^2 \tag{25}$$

where Δa is the measured acceleration uncertainty of $0.046g$. At $t = 0.25$ s, $\Delta w/L$ is ~ 0.015. In an attempt to minimize the effect of this drift, a high-pass filter was used to remove the constant dc component of the acceleration signal. This filtered acceleration signal was then integrated twice in time to derive the tip deflections.

Results

Nonlinear Analysis of Model Beam

An analysis was performed to determine the effect of the nonlinear terms in Eq. (13) on the bending behavior of the model beam. Because all of the nonlinear terms appear in a force vector, a simple static analysis is sufficient to determine their importance to the tunnel-strike phenomenon and drop-test experiment. With this simplification, Eq. (13) reduces to

$$K\tilde{w} = \boldsymbol{F} + \boldsymbol{F}_{NL}(\tilde{w}) \tag{26}$$

A range of distributed vertical loads, scaled in multiples of the acceleration because of gravity, were applied to the model beam. A Newton–Raphson iteration technique was used to

solve Eq. (26) for the flap deflection.[29] Figure 3 compares the calculated linear and nonlinear solutions for the deflection of the model blade tip as a function of the applied distributed load. For a tip deflection 18% of the length of the beam, large enough to result in a tunnel strike and the maximum deflection for the drop tests, the linear and nonlinear deflection theories are almost identical. Note the error between linear and nonlinear deflection theories is less than 4% for a tip deflection 18% of the blade length. Linear bending theory is thus deemed sufficient for both the H-46 tunnel-strike problem and the model beam drop tests. Further correlation with experimental results from Ref. 25 was also performed in Ref. 28.

Modal Convergence Study

To obtain converged natural frequencies and mode shapes for the first six bending modes, a total of 20 finite elements was required. To determine the minimum number of modes for use in each modal space integration technique, a convergence study was performed. The maximum tip deflection and the maximum calculated strain at $x/L = 0.20$ in a drop test from 9.7 deg were examined as convergence parameters. The results of the convergence study are presented in Table 2. After considering the results in Table 2 and examining the transient responses, the modal swapping off technique sufficiently converged for six modes, whereas the modal swapping on technique, because it more accurately represents the boundary conditions at all times, converged for only four modes.

Effect of Structural Damping

Although the structural damping measured in the modal analysis tests is only a few percent of critical, the inclusion of the dissipation has a substantial effect on the transient response of the predicted flap hinge angle and strain of the model blade. Figure 4 shows the response of the flap hinge angle and strain at $x/L = 0.20$, with and without the measured modal damping ratios. The small rebounds of the flap hinge angle off of the droop stop are removed when structural damping is included and the two larger rebounds have decreased in magnitude. An even greater effect can be seen in the predicted strain. The structural damping removes the high-frequency content, and reduces the maximum strain by 20%. The tip deflection response, included in Ref. 28, is not shown here because the effect of the structural damping is very small.

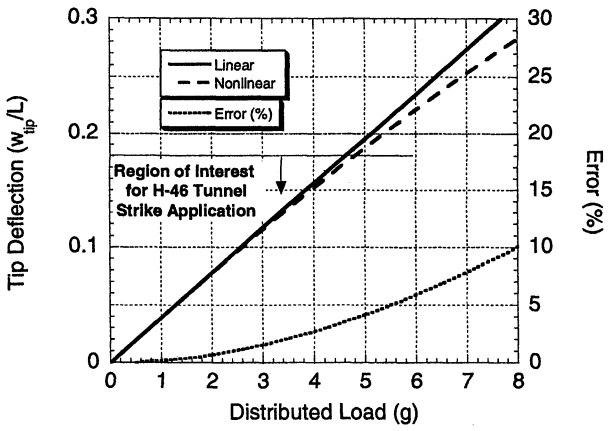

Fig. 3 Nonlinear analysis for model beam.

Example Drop Test

This section will compare the calculated transient responses of the model blade tip deflection, flap hinge angle, and strain with the experimental data generated from a drop test from 9.7 deg. The transient response of the flap hinge angle is shown in Fig. 5. The cause of the sudden upward rotation of the flap hinge angle at $t = 0.10$ s is because the blade flexes while it falls. The experimental data tracks well with the analytical prediction before the impact and while in contact with the droop stop. The rebound of the flap hinge angle predicted to be 5.4 deg by the full finite element space technique, 5.6 deg by the modal swapping off integration technique, and 6.2 deg by the modal swapping on integration technique is actually only 5.1 deg as measured by the linear motion potentiometer.

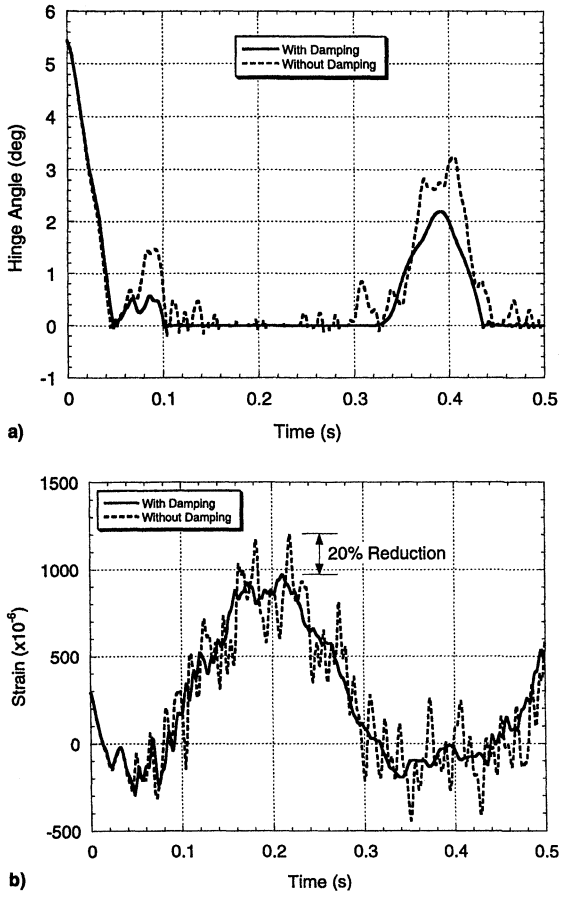

Fig. 4 Effect of structural damping on a) model blade hinge angle and b) model blade strain at $x/L = 0.20$.

Table 2 Modal convergence study

	Predicted tip deflection, w_{tip}/L		Predicted strain, $\times 10^{-6}$	
Number of modes	Modal swapping off	Modal swapping on	Modal swapping off	Modal swapping on
1	0	−0.177	0	1178.3
2	−0.149	−0.171	632.4	1375.8
3	−0.150	−0.172	1283.3	1398.2
4	−0.165	−0.172	1287.3	1388.8
5	−0.167	——	1344.0	——
6	−0.167	——	1329.1	——

This measured rebound also occurs 0.04 s later than the predicted rebound.

The transient response of the tip deflection is shown in Fig. 6. Much like the upward movement of the flap hinge angle, the cause of the upward motion of the blade tip at $t = 0.04$ s is caused by the flexing of the blade while falling. Both the experimental data and analytic predictions capture this phenomenon. The maximum tip deflection, w_{tip}/L, of -0.17 at $t = 0.25$ s for the analytic methods is in good agreement with the experimental data. However, the time at which the measured maximum tip deflection occurs is 0.02 s after the calculated tip deflection. For this specific drop test, the buildup of the uncertainty in the accelerometer measurement is not evident.

The transient response of the strain gauge at $x/L = 0.20$ is shown in Fig. 7. Overall, there is good agreement in the peaks and valleys of the measured and predicted strain. Note that the strain becomes negative at $t = 0.05$ s, indicating the beam is actually curved upward, and is indicative of the blade flexing as it falls. The maximum strain of 1400 microstrain is well captured by the experimental data and analytic predictions; however, the experimental data again lag behind the analytic predictions by 0.02 s.

Experimental Time Lag

A time lag between the experimental data and the analytic predictions exists. This time lag is ~0.02 s at the model beam's point of maximum deflection, and increases to 0.04 s by the end of the drop test. Returning to Table 1, the majority of the predicted natural frequencies are 3–5% higher than the measured natural frequencies. If the flapwise stiffness distribution of the model beam were decreased by 10%, the disparity between the measured and predicted natural frequencies would be nearly eliminated. Figure 8 compares time response of the flap hinge angle and strain at $x/L = 0.20$ for the original beam, the beam with the adjusted natural frequencies, and the experimental data. The time lag between the adjusted beam and the experimental data has been reduced. Also note that amplitude of the main rebound of the flap hinge angle matches the experimental data more closely.

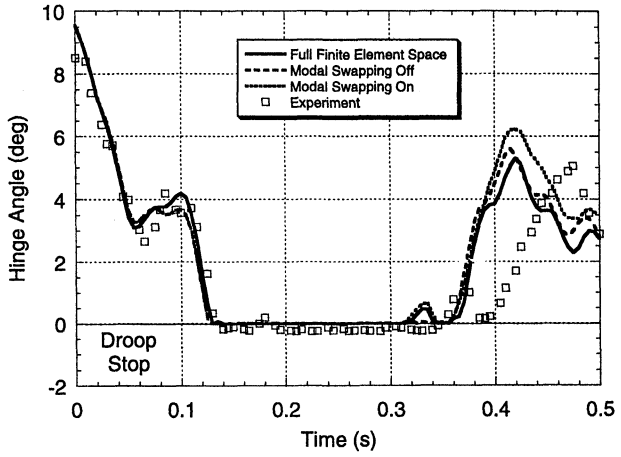

Fig. 5 Model blade hinge angle when dropped from 9.7 deg.

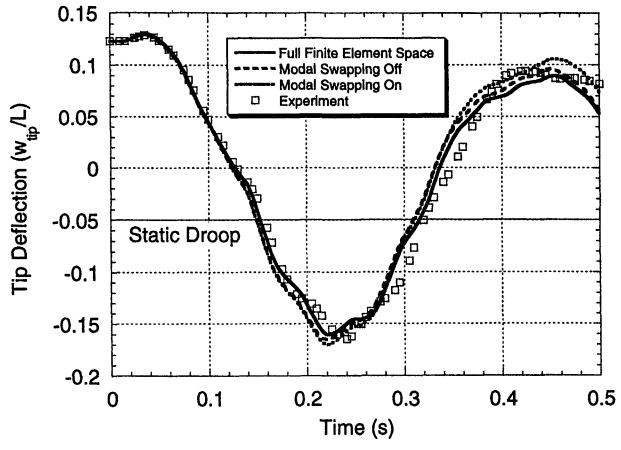

Fig. 6 Model blade tip deflection when dropped from 9.7 deg.

Summary of All Drop Tests

Figure 9 shows the results of the measured and predicted maximum tip deflections for all of the drop tests. The three analytic methods predict almost identical variations in the maximum tip deflection with the initial drop angle. Here, the buildup of uncertainty in the accelerometer measurement can be readily seen. Note the spread in the measured maximum tip deflections for similar initial drop angles. In the worst case, the difference between the measured and predicted maximum

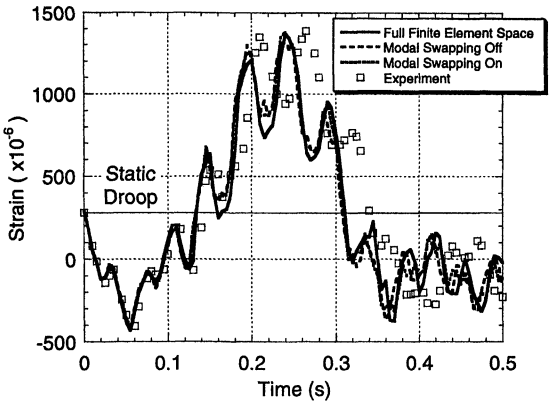

Fig. 7 Model blade strain at $x/L = 0.20$ when dropped from 9.7 deg.

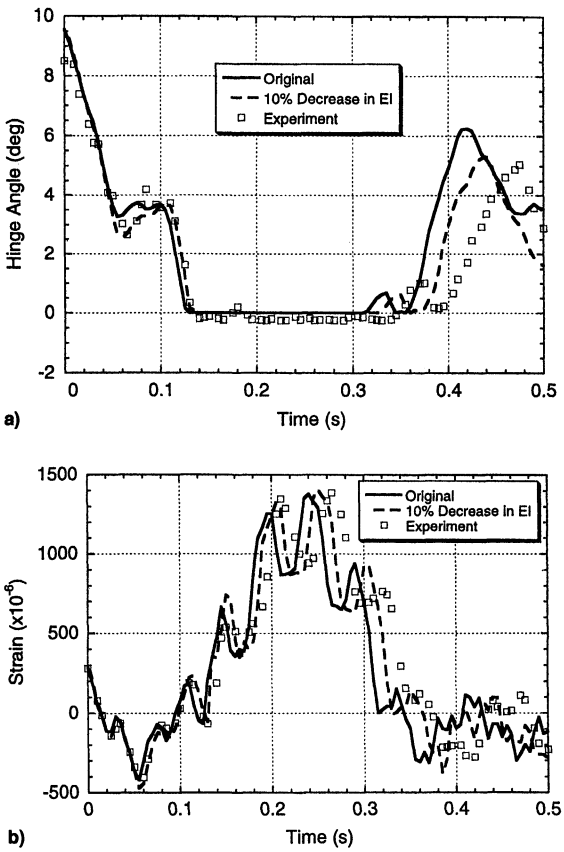

Fig. 8 Effect of matching blade natural frequencies on a) model blade hinge angle and b) model blade strain at $x/L = 0.20$.

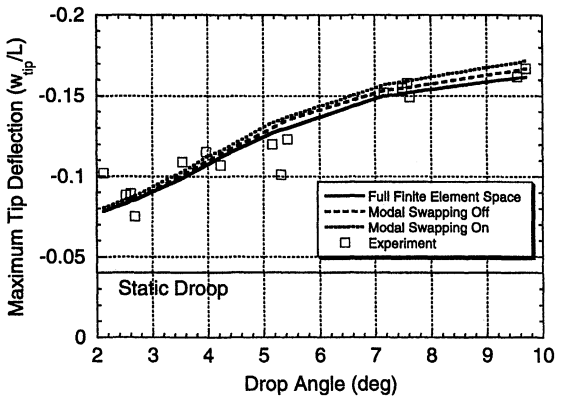

Fig. 9 Maximum tip deflections.

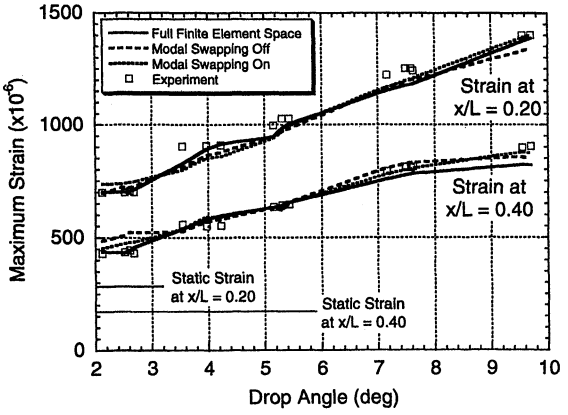

Fig. 10 Maximum strains at x/L = 0.20 and 0.40.

w_{tip}/L is equal to 0.028 from a drop angle of 4.5 deg, an error of 23%. As stated earlier, the uncertainty in the maximum tip deflection can be as large as $\Delta w/L = 0.015$. The maximum tip deflections range from 0.08 for the lowest drop angle to 0.18 for the highest drop angle. Therefore, the error in the maximum tip deflection because of the accelerometer drift can be as large as 19% for the lowest drop angle, to 8% for the highest drop angle.

Figure 10 shows the variation of the maximum strain at x/L = 0.20 and 0.40. The spread in the maximum measured strain for similar drop angles is much lower than the spread for the maximum tip deflections. The variation in the maximum strain was less than 2% for all three strain gauges. This shows that the strain gauge measurements were very repeatable, unlike the tip deflection measurements. The maximum strain measured at x/L = 0.20 in the drop tests is 1400 microstrain, which is almost five times higher than the static strain.

Computational Efficiency

As seen in the previous sections, each of the analytic techniques presented, the full finite element space integration, the modal swapping off integration, and the modal swapping on integration, provide almost identical solutions for each drop test. However, the accuracy and computational efficiency of each solution method are important. Each drop test simulates 0.5 s of real time. The full finite element space solution method requires the most CPU time, a total of 70 s, because 41 degrees of freedom are used. The modal swapping off solution is the next most efficient model, requiring 24 s of CPU time. Instead of integrating 41 coupled equations of motion, only six normal modes are required. The modal swapping on solution is the most efficient of the three analytic methods, requiring only 13 s of CPU time, because only four normal modes were required for the solution.

The differences in CPU time to generate even the longest drop test solution are not very substantial; however, the rotor blade and droop stop impact event is a very small part of a larger picture, the complete rotor engagement and disengagement simulation. Many computationally intensive features such as blade element unsteady aerodynamics, which result in motion-dependent terms and large numbers of degrees of freedom, including flap and torsion in the aeroelastic rotor analysis, make computational efficiency essential. A dramatic difference in CPU time can result using the three integration techniques in the aeroelastic analysis in Refs. 6–9. The full finite element space engagement solution is again the longest, requiring 160 h of CPU time on an RS-6000 workstation. If the engagement simulation is performed using the modal swapping off integration, the size of the problem is reduced to six normal modes. This reduces the length of the simulation to 10 h, which is still fairly substantial. Finally, if the modal swapping on integration is used, only $\frac{1}{2}$ h is required for the engagement simulation.[9] Clearly, when the issue of computational efficiency is considered along with accuracy, the modal swapping on integration is the superior method for use in the rotor engagement/disengagement simulation.

Conclusions

An analysis has been developed using the finite element method, and experiments have been performed with a Froude-scaled model blade to investigate the transient response of a helicopter rotor blade during a droop stop impact event. The following conclusions can be drawn, based on the investigation presented in this paper:

1) For the model blade used in the drop tests, linear beam bending theory was in good agreement with nonlinear theory. For tip deflections up to 18% of the blade length, less than 4% error is incurred by ignoring nonlinear terms.

2) A small amount of measured structural damping, when included with the analysis, was shown to have a significant impact on the flap hinge angle and strain responses. The predicted high-frequency content of each signal was removed and the predicted maximum strain was reduced by 20%.

3) Three different techniques for the time integration of the blade equations of motion were examined. When compared with the experimental data generated in the drop tests, all three methods displayed good correlation. Maximum tip deflections were typically within 10% of the predicted values, whereas maximum strains were predicted within 5% of the predicted values. Upon examining the issue of computational efficiency, the solution method using both unconstrained and constrained modes was found to be the fastest solution method. It most accurately models the change in the boundary conditions of the blade at the time of droop stop impact; therefore, it is the best analytic method for use in an aeroelastic rotor engage/disengage simulation.

4) Most of the time lag between the experimental data and the analytic predictions is caused by the discrepancies between the predicted and measured natural frequencies of the model blade. If the flapwise stiffness is decreased by 10%, the predicted natural frequencies match the measured natural frequencies, and the time lag is greatly reduced.

Acknowledgments

The authors would like to thank the Dynamic Interface Team of the Naval Air Warfare Center at Patuxent River, Maryland; the National Rotorcraft Technology Center; and the U.S. Marine Corps Depot at Cherry Point, North Carolina, for financing this work. The authors would also like to thank George Lesieutre for his helpful observations.

References

[1]Hurst, D. W., and Newman, S. J., "Wind Tunnel Measurements of Ship Induced Turbulence and the Prediction of Helicopter Rotor Blade Response," *Vertica*, Vol. 12, No. 3, 1988, pp. 267–278.

[2]Newman, S. J., "A Theoretical Model for Predicting the Blade Sailing Behaviour of a Semi-Rigid Rotor Helicopter," *Vertica*, Vol. 14, No. 4, 1990, pp. 531–544.

[3]Newman, S. J., "The Application of a Theoretical Blade Sailing Model to Predict the Behaviour of Articulated Helicopter Rotors," *Aeronautical Journal of the Royal Aeronautical Society*, Vol. 96, No. 956, 1992, pp. 233–239.

[4]Newman, S. J., "The Problems of Rotor Engagement and Disengagement of a Shipborne Helicopter," *Journal of Naval Sciences*, Vol. 20, No. 1, 1994, pp. 56–64.

[5]Newman, S. J., "The Verification of a Theoretical Helicopter Rotor Blade Sailing Method by Means of Windtunnel Testing," *The Aeronautical Journal of the Royal Aeronautical Society*, Vol. 99, No. 982, 1995, pp. 41–50.

[6]Geyer, W. P., "Aeroelastic Analysis of Transient Blade Dynamics During Shipboard Engage/Disengage Operations," M.S. Thesis, Dept. of Aerospace Engineering, Pennsylvania State Univ., University Park, PA, Aug. 1995.

[7]Geyer, W. P., "Aeroelastic Analysis of Transient Blade Dynamics During Shipboard Engage/Disengage Operations," *Proceedings of the 2nd International Aeromechanics Specialist's Meeting* (Fairfield County, CT), American Helicopter Society, Alexandria, VA, 1995, pp. 91–114.

[8]Geyer, W. P., Smith, E. C., and Keller, J., "Validation and Application of a Transient Aeroelastic Analysis for Shipboard Engage/Disengage Operations," *Proceedings of the 52nd Annual National Forum of the American Helicopter Society* (Washington, DC), American Helicopter Society, Alexandria, VA, 1996, pp. 152–167.

[9]Geyer, W. P., Smith, E. C., and Keller, J. A., "Aeroelastic Analysis of Transient Blade Dynamics During Shipboard Engage/Disengage Operations," *Journal of Aircraft*, Vol. 35, No. 3, 1998, pp. 445–453.

[10]Vetter, D. R., Groulx, J. W., and Carico, G. D., "H-46 Rotor Engage/Disengage Evaluation Aboard USS-GUADALCANAL (LPH-7) Final Report," Naval Air Test Center, Rept. FT-49R-74, Patuxent River, MD, March 1974.

[11]Ball, J. C., and White, W. R., "H-46 Dynamic Interface Tests Aboard USS GUAM (LPH-9)," Naval Air Test Center, Rept. RW-28R-83, Patuxent River, MD, June 1984.

[12]Hurley, G. E., Pittman, C. W., and Trick, L. L., "HH-46/CV-64 Rotor Engage/Disengage Test," Naval Air Test Center, Rept. RW-55R-84, Patuxent River, MD, Oct. 1984.

[13]Narveson, M. L., "Flow Modification over a Backward Facing Step," M.S. Thesis, Dept. of Aeronautical Engineering, Naval Postgraduate School, Monterey, CA, Sept. 1990.

[14]Val Healy, J., "The Prospects for Simulating the Helicopter/Ship Interface," *Naval Engineers Journal*, Vol. 99, No. 2, 1987, pp. 45–63.

[15]Leone, P. F., "Theoretical and Experimental Study of the Flap Droop Stop Impact Transient Aero-Elastic Response of a Helicopter Rotor Blade," *Journal of the American Helicopter Society*, Vol. 9, No. 1, 1964, pp. 32–37.

[16]Fathi, F., and Popplewell, N., "Improved Approximations for a Beam Impacting a Stop," *Journal of Sound and Vibration*, Vol. 170, No. 3, 1994, pp. 365–375.

[17]Lo, C. C., "A Cantilever Beam Chattering Against a Stop," *Journal of Sound and Vibration*, Vol. 69, No. 2, 1980, pp. 245–255.

[18]Molnar, A. J., Vashi, K. M., and Gay, C. W., "Application of the Normal Mode Theory and Pseudoforce Methods to Solve Problems with Nonlinearities," *Journal of Pressure Vessel Technology*, Vol. 98, May 1976, pp. 151–156.

[19]Shah, V. J., Bohm, G. J., and Nahavandi, A. N., "Modal Superposition Method for Computationally Economic Nonlinear Structural Analysis," American Society of Mechanical Engineers, Paper 78-PVP-70, New York, 1978.

[20]Davies, H. G., and Rogers, R. J., "The Vibration of Structures Elastically Constrained at Discrete Points," *Journal of Sound and Vibration*, Vol. 63, No. 3, 1979, pp. 437–447.

[21]Chen, S. S., Rosenberg, G. S., and Wambsganss, M. W., "On Tube-Baffle Impact During Heat Exchanger Tube Vibration," *Journal of Mechanical Engineering Science*, Vol. 12, 1970, pp. 27–35.

[22]Rogers, R. J., and Pick, R. J., "Factors Associated with Support Plate Forces Due to Heat-Exchanger Tube Vibratory Contact," *Nuclear Engineering and Design*, Vol. 44, No. 2, 1977, pp. 247–253.

[23]Rogers, R. J., and Pick, R. J., "On the Dynamic Spatial Response of a Heat Exchanger Tube with Intermittent Baffle Contacts," *Nuclear Engineering and Design*, Vol. 36, No. 1, 1976, pp. 81–90.

[24]Shaw, S. W., "Forced Vibrations of a Beam with One-Sided Amplitude Constraint: Theory and Experiment," *Journal of Sound and Vibration*, Vol. 99, No. 2, 1985, pp. 199–212.

[25]Walker, A. C., and Hall, D. G., "An Analysis of the Large Deflections of Beams Using the Rayleigh-Ritz Finite Element Method," *Aeronautical Quarterly*, Vol. 19, Nov. 1968, pp. 357–367.

[26]Keller, J. A., "An Experimental and Theoretical Correlation of an Analysis for Helicopter Rotor Blade and Droop Stop Impacts," M.S. Thesis, Dept. of Aerospace Engineering, Pennsylvania State Univ., University Park, PA, Dec. 1997.

[27]Rao, S. S., *Mechanical Vibrations*, 3rd ed., Addison–Wesley, Reading, MA, 1995, pp. 712, 713.

[28]Keller, J. A., Smith, E. C., and Knarr, C. R. "Experimental/Theoretical Correlation of Analysis for Helicopter Rotor Blade/Droop Stop Impacts," *Proceedings of the AIAA/ASME/ASCE/AHS/ASC 38th Structures, Structural Dynamics, and Materials Conference* (Kissimmee, FL), AIAA, Washington, DC, 1997, pp. 345–357.

[29]Kreyszig, E., *Advanced Engineering Mathematics*, 6th ed., Wiley, New York, 1988, pp. 952, 953.